JOURNAL OF APPLIED PHYSICS **115**, 184305 (2014)

Dielectric spectroscopy at the nanoscale by atomic force microscopy: A simple model linking materials properties and experimental response

Luis A. Miccio,[1,2,3,a)] Mohammed M. Kummali,[1,3] Gustavo A. Schwartz,[1,2] Ángel Alegría,[1,3] and Juan Colmenero[1,2,3]
[1]*Centro de Física de Materiales (CSIC-UPV/EHU), P. M. de Lardizabal 5, 20018 San Sebastián, Spain*
[2]*Donostia International Physics Center, P. M. de Lardizabal 4, 20018 San Sebastián, Spain*
[3]*Departamento de Física de Materiales (UPV/EHU), 20080 San Sebastián, Spain*

(Received 18 February 2014; accepted 29 April 2014; published online 13 May 2014)

The use of an atomic force microscope for studying molecular dynamics through dielectric spectroscopy with spatial resolution in the nanometer scale is a recently developed approach. However, difficulties in the quantitative connection of the obtained data and the material dielectric properties, namely, frequency dependent dielectric permittivity, have limited its application. In this work, we develop a simple electrical model based on physically meaningful parameters to connect the atomic force microscopy (AFM) based dielectric spectroscopy experimental results with the material dielectric properties. We have tested the accuracy of the model and analyzed the relevance of the forces arising from the electrical interaction with the AFM probe cantilever. In this way, by using this model, it is now possible to obtain quantitative information of the local dielectric material properties in a broad frequency range. Furthermore, it is also possible to determine the experimental setup providing the best sensitivity in the detected signal. © *2014 AIP Publishing LLC*. [http://dx.doi.org/10.1063/1.4875836]

I. INTRODUCTION

During the last decades, broadband dielectric spectroscopy (BDS) has shown to be a very useful technique in the study of the molecular dynamics of insulating materials. The huge frequency range achieved (10^{-5}–10^{12} Hz) and the possibility of measuring under different temperature, pressure, and environmental conditions, allow the observation of a large variety of processes with very different time scales. Within this extraordinary experimental window, molecular and collective dipolar fluctuations, charge transport and polarization effects take place, in turn determining the dielectric response of the material under study.[1]

In the last years, the growing interest in nanostructured materials highlighted the need of measurements providing local material properties. However, BDS cannot provide direct information of these local features, due to the lack of spatial resolution.

On the other hand, atomic force microscopy (AFM) provides outstanding spatial resolution of materials surface.[2,3] In particular, electric force microscopy (EFM)[4–10] can be used for detecting local electrical interactions within these materials. Recently, AFM has been used as the basis to develop local dielectric spectroscopy (LDS).[11] Within this approach, the electrical interaction resulting by applying an AC voltage to a conductive AFM probe is used to reveal information about the dielectric relaxation processes within the material at local scale. Therefore, this technique combines the capability of sensing the molecular dynamics with the outstanding spatial resolution of AFM. These measurements are based on a phase locked loop (PLL) setup[11–14] and detect the force gradient. In addition, a method based on the detection of the force was also recently developed, the so called nanoDielectric Spectroscopy (*n*DS).[15,16]

As the detection in AFM based dielectric experiment relies on the photodiode, the measured parameters are always associated to the cantilever oscillation mechanics. In particular, in the force detection method, the measured parameters are directly the root mean square (RMS) oscillation amplitude, $|V_{Ph}|$, and the phase, θ, of the photodiode signal. However, the connection between the complex dielectric permittivity of the material under study (namely $\varepsilon^*(f) = \varepsilon'(f) - i\,\varepsilon''(f)$) and the output signals of a *n*DS experiment is not so straightforward. Thus, in order to explicitly establish this connection, a physical model describing *n*DS experiments is necessary. Although mathematical descriptions of the electrical interaction between an AFM probe (upper electrode) and a metallic lower electrode have been established[17,18]—including the presence of a dielectric layer between the electrodes[19,20]—to the best of our knowledge no such studies related to the electrical phase and amplitude of force detection-based dielectric spectroscopy have been done.

In order to successfully describe the dielectric losses in local dielectric measurements, it is necessary to consider the effect of the dielectric relaxations on the mechanical oscillation of the cantilever. Thus, by expressing the force on the probe as a function of the dielectric properties of a given material, a mathematical description of the cantilever RMS oscillation amplitude and phase for any electrical excitation frequency can be carried out.

In this work, we propose a simple model to relate the output of AFM based dielectric spectroscopy experiments with the electrical properties of the sample, based on the

[a)]Author to whom correspondence should be addressed. Electronic mail: luisalejandro_miccio@ehu.es

 © 2014 AIP Publishing LLC

[This article is copyrighted as indicated in the article. Reuse of AIP content is subject to the terms at: http://scitation.aip.org/termsconditions. Downloaded to] IP: 161.111.180.191 On: Mon, 29 Sep 2014 09:04:52

cantilever mechanics and the electrical interaction of the different parts of the probe. In a first step, we develop an equivalent circuit model and the oscillation amplitude expressions for the AFM probe. In a second step, we compare the data obtained from the model with a gold surface (dissipation free sample) and with a typical polymer film supported on it. As a third step, we use the model to analyze the dependence of the detected signal with the experimental parameters, and thereby determine optimum conditions for the measurements. Finally, in a fourth step, these predictions are evaluated by using special AFM probes. Therefore, here we present a physically meaningful model in order to quantitatively connect the signal detected in AFM based dielectric spectroscopy measurements with the dielectric material properties.

II. THEORETICAL BACKGROUND

The EFM is based on the electrical force (F_e) resulting from the interaction of a conductive AFM probe with charged and/or polarizable entities in the material.[5,6,18–23] F_e can be evaluated by modeling the tip-sample system as a capacitor (capacitance C): when a voltage (V) is applied, the resulting electrostatic potential energy is $W = {}^1\!/_2 CV^2$ and the corresponding electrostatic force acting on the tip $F_e = dW/dz$ (being z the coordinate along which the tip-sample distance is measured). Consequently, when a sinusoidal voltage $[V(t) = V_0 \sin(\omega_e t)]$ of frequency $f_e = \omega_e/2\pi$ is applied to the AFM probe, the corresponding force is a sinusoidal function given by

$$F_e(t) = \frac{1}{2}\frac{\partial C}{\partial z}[V_S + V_{DC} + V_0 \sin(\omega_e t)]^2, \tag{1}$$

where V_S is the surface potential and V_{DC} is the applied DC voltage (if any).[15] $F_e(t)$ has one component at a frequency double than that used in the excitation due to the quadratic relationship between F_e and V

$$F_{2\omega_e}(t) = -\frac{1}{4}\frac{\partial C}{\partial z}V_0^2 \cos(2\omega_e t). \tag{2}$$

The force amplitude and phase for this component depend both on the experimental conditions and on the dielectric properties of the material under investigation. Therefore, by detecting the component of the probe motion at a frequency double of the electrical excitation frequency, information about the local dielectric relaxations of the materials under investigation can be obtained. These measurements (nDS) require the analysis of the signal from the AFM photodiode with a Lock-In Amplifier (LIA) in order to obtain both the amplitude $|V_{Ph}|$ and electric phase θ of the cantilever oscillations at $2\omega_e$ (in this way, any component of the force at different frequencies is filtered). In the case of a loss-free dielectric material, the signal amplitude brings information on the static dielectric permittivity, which is frequency independent. However, when dielectric relaxations take place in a material, the dielectric permittivity becomes frequency dependent and correspondingly a dielectric loss process will appear (which in turn results in a complex capacitance) in Eq. (2), which then becomes

$$F^*_{2\omega_e}(t) = -\frac{1}{4}\frac{\partial C^*}{\partial z}V_0^2 \cos(2\omega_e t). \tag{3}$$

Typically, a nDS experiment is performed at a single location of the sample by employing the so called double-pass method (DPM), where the measurements are performed in two steps. In a first step, the sample topography is precisely established in a standard "Tapping" mode experiment. Subsequently, in lift mode, the mechanical cantilever excitation is set to zero, in order to maintain a constant tip-sample distance, and the probe motion generated by the tip-sample interaction due to the application of an alternating voltage is analyzed by the LIA. Thus, the LIA simultaneously provides both the RMS oscillation amplitude ($|V_{Ph}|$) and the electrical phase (θ) of the cantilever response at $2\omega_e$. A reference experiment on a dissipation free sample is performed for each probe in order to precisely establish the reference electric phase (θ_{ref}) (the phase associated with the electronics and the mechanical characteristics of the AFM probe). Subsequently, the dielectric spectra are obtained by plotting the phase shift ($\Delta\theta$), obtained by subtracting the reference phase (θ_{ref}) from the original sample response (θ), as a function of the electrical excitation frequency.

III. MODEL

In this section, we describe the modeling of the experimental setup of *nano*Dielectric Spectroscopy. In a first step, the effective capacitance between the AFM probe and the lower electrode is defined by considering separately the contributions from the three parts of the AFM probe: apex of the tip, cone, and cantilever. Once these capacitances are known, the force acting on the probe is numerically obtained from Eq. (3). In the second step, expressions for the phase and the oscillation amplitude are obtained by considering the cantilever as a damped harmonic oscillator.

A. Geometry

The geometry of the different elements for AFM based dielectric spectroscopy can be well described by the scheme shown in Figure 1. As shown, the AFM probe acting as upper electrode is composed by three parts: (1) a cantilever of length L, width W, and angle α (Figure 1(a)); (2) a cone of height H, base of diameter B, and angle β (Figure 1(b)); and (3) an spherical apex of radius R at the end of the cone (not shown). On the other hand, the lower electrode is a flat grounded gold sputtered metallic disc. As shown in Figure 1(a), the space between electrodes is partially filled with a polymer film (i.e., sample under study) of thickness h.

B. Capacitance and force expressions

The electrical interaction of the AFM probe with the polymer sample and the grounded lower electrode is modeled by using the equivalent circuit shown in Figure 1(f) (where C_1 and C_2 stand for cantilever-air and cantilever-polymer capacitances; C_3 and C_4 stand for cone-air and cone-polymer capacitances; and C_5 stands for apex-air and apex-polymer capacitances).

[This article is copyrighted as indicated in the article. Reuse of AIP content is subject to the terms at: http://scitation.aip.org/termsconditions. Downloaded to] IP: 161.111.180.191 On: Mon, 29 Sep 2014 09:04:52

The effective cantilever capacitance $C^*_{cantilever}$ (C_1 and C_2, in Figure 1(f)) is obtained by considering a parallel plate capacitor (of area $A_{cantilever}$) for the polymer and a non-parallel plate capacitor for the air (Figure 1(e))

$$C^*_{cantilever} = \left[f_{BE}(z+H) \cdot \left(\frac{\varepsilon_0 \cdot W}{\tan(\alpha)} \cdot \ln\left(1 + \frac{L \cdot \sin(\alpha)}{z+H}\right)\right)^{-1} + \left(\frac{\varepsilon_o \cdot \varepsilon^* \cdot A_{cantilever}}{h}\right)^{-1}\right]^{-1}. \tag{4}$$

The border effects were introduced through a factor f_{BE} affecting the capacitance expression.[24] Cone effective capacitance, C^*_{cone}, is also obtained by considering air and polymer contributions separately. The expression for the cone-air capacitance (C_3 in Figure 1(f)) arises from the integration of concentric disks, as shown in Figure 1(c), while cone-polymer capacitance is obtained by considering a disk shaped parallel plate capacitor of thickness h and area $A_{cone}(z)$, as schemed in Figure 1(d). In this case, the border effects were introduced directly in the integration process as a function of position ($\boldsymbol{f_{BE}}(z) = \boldsymbol{m}_0 \cdot \boldsymbol{z} + \boldsymbol{n}_0$). The resultant expression is shown below:

$$\begin{aligned} C^*_{cone} &= \left[(\varsigma_1 + \varsigma_2 + \varsigma_3)^{-1} + \left[\frac{\varepsilon_0 \cdot \varepsilon^* \cdot A_{cone}(z)}{h}\right]^{-1}\right]^{-1} \\ \varsigma_1 &= \frac{\varepsilon_0 \cdot \pi \cdot m_0}{\tan(\beta)^2} \cdot \left(\frac{B}{2} - R\right) \\ \varsigma_2 &= \frac{\varepsilon_0 \cdot \pi \cdot n_0}{\tan(\beta)^3} \cdot \left(\frac{B}{2} - R\right) \\ \varsigma_3 &= \frac{\varepsilon_0 \cdot \pi \cdot n_0}{\tan(\beta)^3} \cdot \left(z \cdot \ln \frac{z + \frac{R}{\tan(\beta)}}{z + \frac{B}{2 \cdot \tan(\beta)}} \right). \end{aligned} \tag{5}$$

Finally, the effective apex capacitance is represented by means of Eq. (6)[17,20]

$$C^*_{apex} = 2\pi \cdot \varepsilon_0 \cdot R^2 \left[1 + \frac{R \cdot (1 - \sin\theta_0)}{z + \frac{h}{\varepsilon^*}} \right]. \tag{6}$$

The total force acting on the AFM probe is numerically obtained from the previous capacitances according to Eq. (2). Therefore, with this (probe-sample configuration) AFM setup (Figure 1) it is possible to distinguish three force contributions: (1) the force produced by the apex, (2) the force produced by the cone, and (3) the force produced by the cantilever. As a result, both real and imaginary parts of the total force can be separately analyzed.

C. Oscillation amplitude and phase

Once the force acting on the probe is known, an approximated expression for the cantilever oscillation amplitude can be obtained by assuming a harmonic oscillator behavior.[25] This assumption is rather accurate for this kind of experiments, where cantilever oscillation amplitude is substantially low in comparison with the probe-sample distance (and the driving force dependence with z can be safely neglected). The phase of the cantilever oscillation signal with respect to the excitation is obtained by considering the real and imaginary parts of the damped harmonic oscillator amplitude. As stated before, apex, cone, and cantilever contributions are separately included in a single expression

$$\theta = \tan^{-1}\left[\frac{im(Osc^*_{cantilever}) + im(Osc^*_{cone}) + im(Osc^*_{apex})}{re(Osc^*_{cantilever}) + re(Osc^*_{cone}) + re(Osc^*_{apex})}\right], \tag{7}$$

where $Osc^*_{cantilever}$, Osc^*_{cone}, and Osc^*_{apex} stand for the oscillation amplitude contribution from cantilever, cone, and apex, respectively.

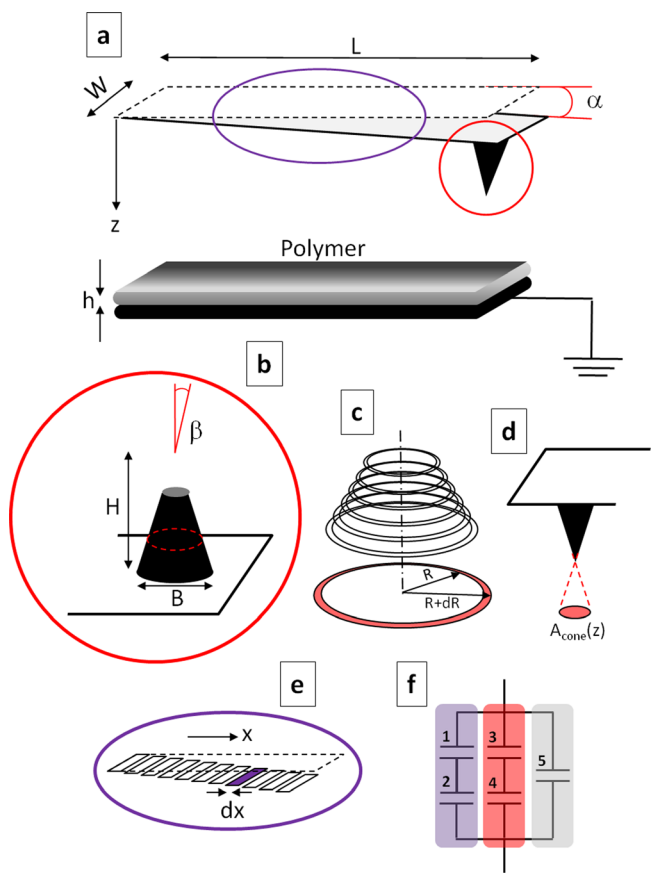

FIG. 1. Geometry of the cantilever-cone-apex/sample system for AFM-based dielectric spectroscopy. (a) General scheme. (b) Zoom of the cone. (c) Scheme of the integration of the cone capacitance. (d) Projected cone area. (e) Scheme of the integration of the cantilever capacitance. (f) Equivalent circuit model in *n*DS.

[This article is copyrighted as indicated in the article. Reuse of AIP content is subject to the terms at: http://scitation.aip.org/termsconditions. Downloaded to] IP: 161.111.180.191 On: Mon, 29 Sep 2014 09:04:52

IV. RESULTS AND DISCUSSION

A. Model validation

In order to validate the proposed model, we employed poly(vinyl acetate) (PVAc), a polymer with a prominent dielectric relaxation detectable close to room temperature—the so called α-relaxation. In a first step, we dielectrically characterized the bulk polymer by means of BDS. In a second step, we measured a film of this polymer by using *n*DS. The thickness was set to about 350 nm, where literature data evidenced no thickness dependency on the α-relaxation,[16,26–29] i.e., we should observe the same α-relaxation dielectric response by both techniques. We then fixed the polymer dielectric relaxation characteristics and used the here proposed model to fit the obtained *n*DS data, leaving as fitting parameters the apex radius, cone angle and cone base diameter, among others. Finally, we independently measured these parameters by using AFM and/or scanning electron microscopy (SEM) to test the model accuracy. This process was repeated for both *n*DS signals, θ and $|V_{ph}|$.

BDS characterization: Figure 2 shows the real and imaginary parts of the complex dielectric permittivity (ε' and ε'', respectively) plotted as a function of frequency for bulk PVAc, at temperatures ranging from 318 K to 373 K (experimental details can be found in Appendix). A Havriliak-Negami (HN) function[30]

$$\varepsilon^* = \varepsilon_\infty + \Delta\varepsilon \cdot \left[1 + (i\omega\tau_{HN})^{\alpha_{HN}}\right]^{-\beta_{HN}} \tag{8}$$

was employed for the fitting procedures, as usual for this kind of relaxations.[1,31,32] Five HN fitting parameters were obtained from the experimental curves at each temperature, α_{HN} and β_{HN} (shape), $\Delta\varepsilon$ (intensity), τ_{HN} (relaxation time), and ε_∞ (high frequency permittivity).

nDS characterization: PVAc polymer films were measured by means of *n*DS at three different temperatures, where PVAc α-relaxation is detectable within the current experimental frequency window. As stated above, film thicknesses were set to about 350 nm, and therefore the alpha relaxation measured by *n*DS can be safely compared with its BDS counterpart (i.e., the previously obtained HN parameters can be used to describe the segmental relaxation in the polymer films). Therefore, HN parameter values were used in the model to describe the polymer relaxation within the studied temperature range.

Figure 3(a) shows the phase shift peaks originated by the dielectric relaxation on the PVAc sample. As expected, there is a shift of the whole peak to higher frequencies as the

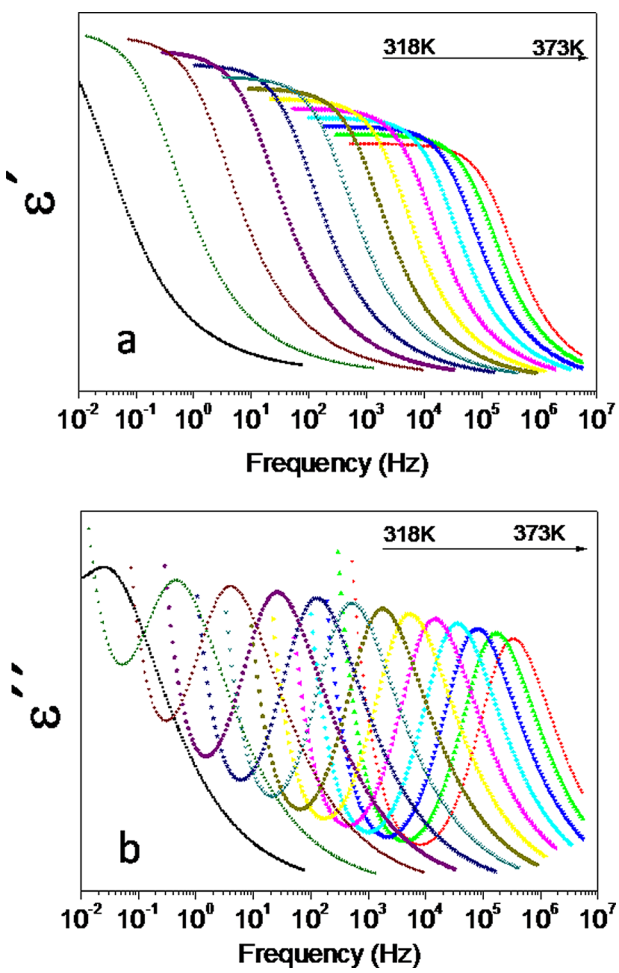

FIG. 2. (a) Real part of the PVAc complex dielectric permittivity (ε') plotted as a function of frequency. (b) Imaginary part of the PVAc complex dielectric permittivity (ε'') plotted as a function of frequency. The results were obtained through BDS for temperatures ranging from 318 K to 373 K.

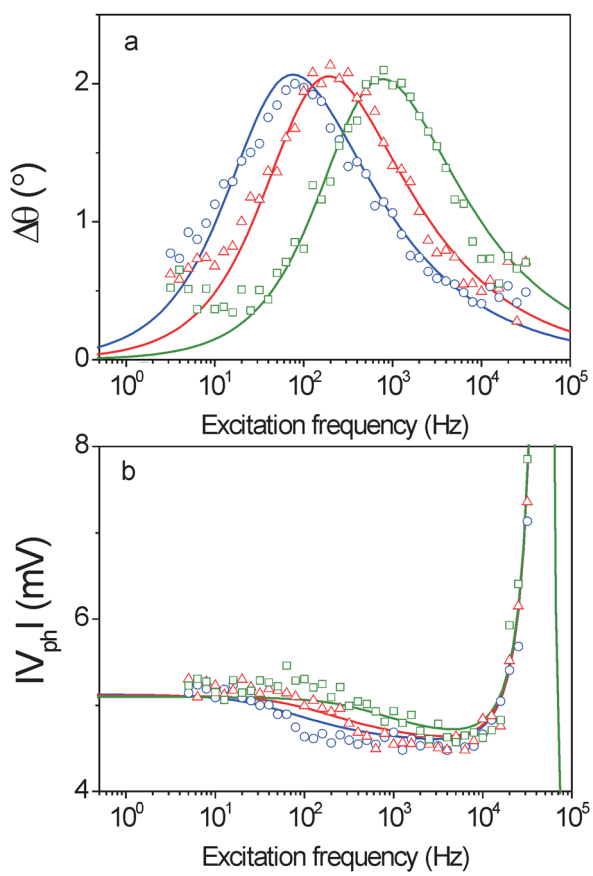

FIG. 3. *n*DS experiments on pure PVAc. The symbols and the lines stand for the experimental results and the fitting output, respectively. (a) Electrical phase as a function of excitation frequency. (b) $|V_{Ph}|$ as a function of excitation frequency. The experimental temperatures are 331, 334, and 339 K for blue, red, and green data sets, respectively.

[This article is copyrighted as indicated in the article. Reuse of AIP content is subject to the terms at: http://scitation.aip.org/termsconditions. Downloaded to] IP: 161.111.180.191 On: Mon, 29 Sep 2014 09:04:52

temperature increases. Intensity and full width at half maximum (FWHM) are nearly the same for the three temperatures.

Lines in Figure 3(a) stand for the fitting results of the proposed model. These fittings were performed simultaneously for the three datasets, and apex radius, tip-sample distance, cantilever angle, cone angle, cone base diameter were left as free parameters. The so obtained values were $R = 24.8$ nm, $z_0 = 22.2$ nm, $B = 11.9\,\mu$m, $\alpha = 10°$, and $\beta = 15°$.

The rest of the parameters of the model were fixed during the fitting procedure to the values obtained by direct measuring (either by employing AFM or SEM for that purpose). In addition, cone angle, cone base diameter, and tip sample distance were also independently measured to obtain a rough first validation of the fitting results.

The cantilever length and width were found to be about 250 μm and 30 μm (SEM). A cone height of 12 μm and an angle of 15° were also determined by SEM. A typical tip-sample distance during experiments of about 23 nm was also found (for more details see Appendix), which is in close agreement with the value obtained from the fitting (about 25 nm).

As stated before, in a *n*DS experiment, the RMS oscillation amplitude is obtained in addition to the electrical phase. Therefore, it is possible to perform an additional validation of the previously obtained parameters by also fitting $|V_{ph}|$ results. Figure 3(b) shows the experimental $|V_{ph}|$ results (symbols) and the corresponding fitting (lines). In this case, the photodiode sensitivity (χ) and the cantilever spring constant (k) were the only free parameters. The obtained values are 16.4 mV/nm and 3 N/m, respectively. Apex radius, tip-sample distance, cone height, and cantilever dimensions were fixed from the previous fitting. As shown, the model output is in close agreement with the experimental data.

In order to further confirm this second fitting procedure, both sensitivity and spring constant were independently measured by using the AFM (through force-distance curves and thermal noise method,[25] respectively). The obtained values 18.6 mV/nm and 2.7 N/m, respectively, are in close agreement with the fitting results.

The obtained results show that the proposed model successfully describes *n*DS experiments, therefore setting a connection between the material dielectric properties and the AFM parameters.

B. Model predictions

In this section, we use the above validated model to study the influence of the experimental setup on *n*DS output. In particular, we focus our attention on the influence of the polymer film thickness in the detected phase shift.[15]

1. Contributions to the nDS phase

Apart from the spatial resolution, one of the most important points of AFM based dielectric spectroscopy is the possibility of studying thin samples and the thickness effects on

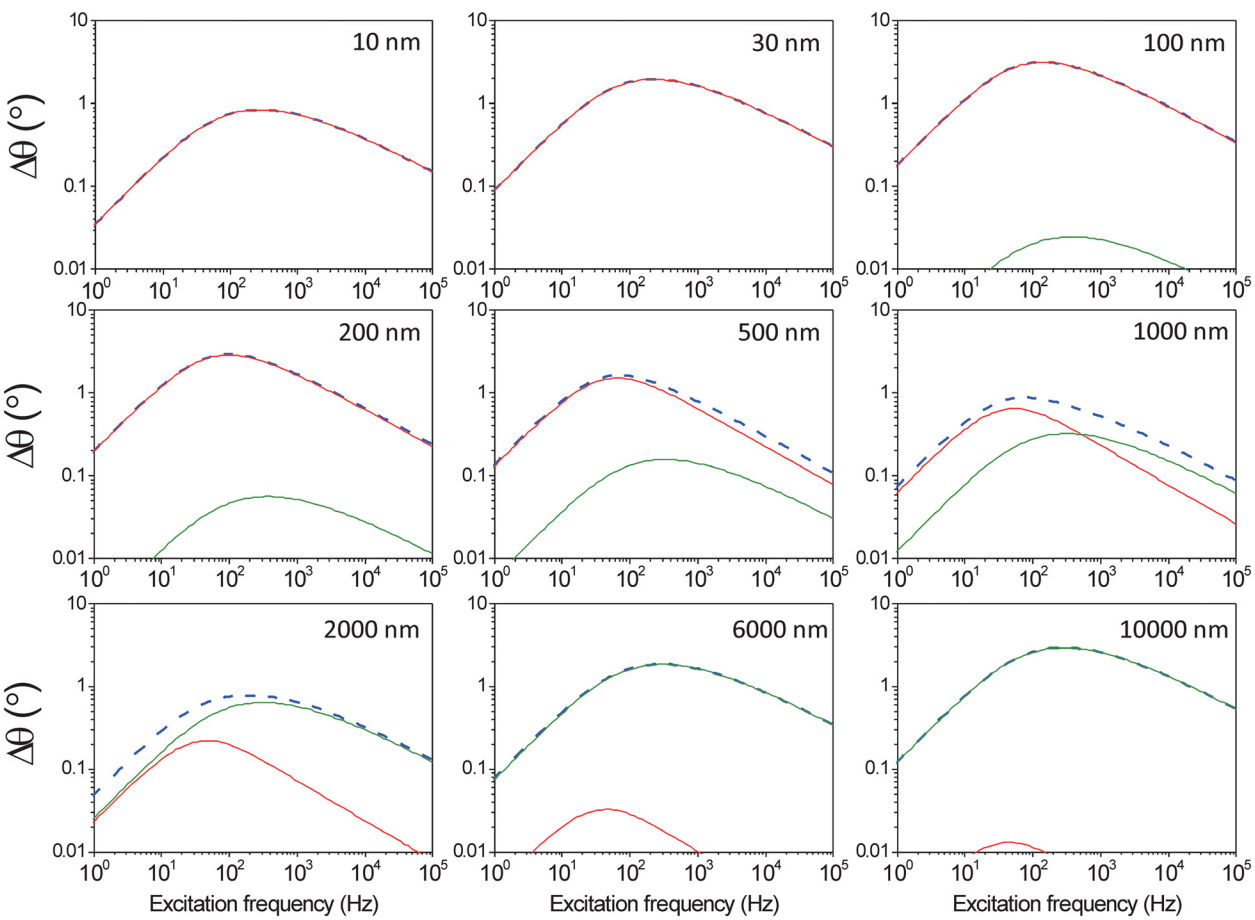

FIG. 4. Electrical phase predicted by the model for different polymer thicknesses. Apex and cantilever contributions to the signal are shown as red and green lines, respectively, while total signal is shown in blue (dashed line). Cone imaginary contribution does not appear in this scale.

[This article is copyrighted as indicated in the article. Reuse of AIP content is subject to the terms at: http://scitation.aip.org/termsconditions. Downloaded to] IP: 161.111.180.191 On: Mon, 29 Sep 2014 09:04:52

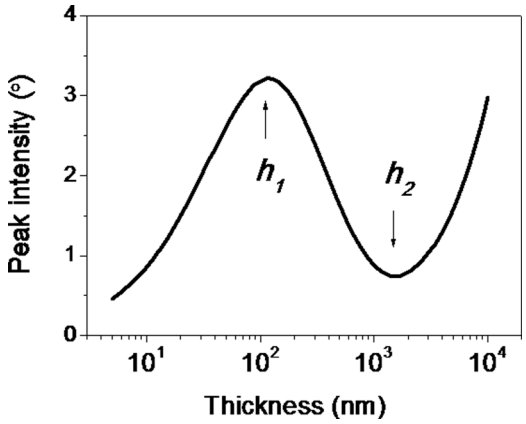

FIG. 5. Peak intensity predicted by the model as a function of the polymer thickness. h_1 and h_2 stand for the thicknesses at the maximum and the minimum of the curve, respectively.

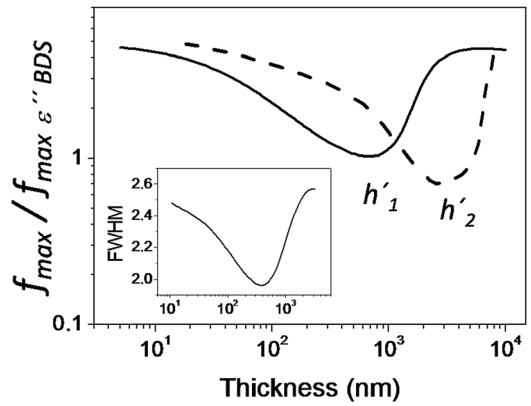

FIG. 6. Frequency of the maximum (of the electrical phase peak) predicted by the model as a function of the polymer thickness. The values were normalized to the frequency of the maximum in ε'' (obtained by BDS). The solid line stands for the force approach, while the dashed line stands for the force gradient mode. h_1' and h_2' stand for the thicknesses at the minimum of the curves. Inset: Full width at half maximum (decades) predicted by the model as a function of the polymer thickness.

the polymer relaxation. However, in *n*DS measurements, the direct influence of thickness on the measured signals, and especially on the characteristics of the observed phase shifts, is also a key factor. Figure 4 shows the model predictions at 331 K (based on the previously obtained parameters) for PVAc films with thicknesses ranging from 10 nm to 10 μm. Apex and cantilever contributions to the signal are shown as red and green lines, respectively, while total signal is shown with a blue (dashed) line. Although the cone signal is considered in the calculations, it is out of scale in Figure 4. This point is further discussed below.

From the analysis of the peak intensity (i.e., the maximum phase shift detected) at each thickness, it is possible to observe a clear trend (Figure 5). At low thicknesses (namely 10 nm to 100 nm), the peak intensity increases as the thickness increases (as already reported in literature,[15] until a maximum is achieved at $h_1 = 100$ nm. The peak intensity then decreases with increasing thicknesses up to $h_2 = 2000$ nm. Finally, at even higher thicknesses, the intensity increases monotonically in the analyzed range. These results will be further discussed below.

Concerning to the frequency of the peak maximum (f_{max}), Figure 6 shows f_{max} normalized to the frequency of the maximum in ε'' obtained from BDS ($f_{max}/f_{max\ \varepsilon''\ BDS}$), as a function of thickness at the same temperature. It is noteworthy that for the typical thin samples, the AFM measured electrical phase shift is approximately proportional to the loss part of the force (material-related signal), thus justifying the comparison with bulk ε'' peak frequency values. This is because a large part of the real component of the force comes from the frequency independent air-related capacitances. For low and medium thicknesses (below 700 nm), f_{max} value decreases monotonically as the thickness increases. These results can be rationalized by considering that at low thicknesses the capacitance related with the gap between the apex and the sample is very relevant. As thickness increases, this effect diminishes until the space between apex and lower electrode is mainly filled by the sample (as it can be seen in the apex curve in Figure 4). However, above 700 nm this tendency is reverted, due to the air gap in the cantilever capacitance.

Finally, the shape of the observed *n*DS peaks was characterized through the study of the FWHM parameter. Like for the previous parameters, FWHM is strongly affected by sample thickness. As shown in Figure 6 inset, the observed trend is closely related to the one observed in f_{max}.

The complex behavior shown by these results evidences the relevance of the different parts of the AFM probe on the detected peaks. As observed in Figure 4, apex contribution clearly dominates the phase shift (nearly coincides with blue line) at low and medium thicknesses (namely 10 nm to 500 nm). At first, phase intensity increases (10 nm to 100 nm) due to the increasing amount of polymer, as already reported.[15] However, for thicknesses higher than 100 nm, the peak intensity starts decreasing, due to the increasing contribution to the real part of the cone and cantilever. These contributions are mostly originated in the air filled cone and cantilever capacitors, due to the fact that the polymer contribution through these parts is completely negligible (in this range of thicknesses).

Above 1000 nm, also the imaginary part of the cantilever capacitance starts contributing to the total signal (it can be seen in Figure 4 that the losses from the apex, red line, do no longer coincide with the blue line). For thicknesses above 2000 nm, the cantilever is responsible for the detected phase shifts. In this thickness range, the spatial resolution is lost, and the signal increases significantly due to the fact that the polymer film fills an increasing fraction of the capacitor. It is worth noticing that cone imaginary contribution never dominates the detected signal (it is first masked by apex signal, and later by cantilever).

In summary, not only the relaxation characteristics of investigated material could affect the properties of the observed phase shift peaks, there is also a clear contribution of the experimental conditions. Furthermore, any experimental result has to be considered as the convolution of the signals related to the different parts of the AFM probe. Therefore, it is of utmost importance to design the appropriate experiment in order to maximize the sensitivity, as well as to obtain reliable measurements.

[This article is copyrighted as indicated in the article. Reuse of AIP content is subject to the terms at: http://scitation.aip.org/termsconditions. Downloaded to] IP: 161.111.180.191 On: Mon, 29 Sep 2014 09:04:52

2. Extension to force gradient approach

The same model here introduced can be used for the analysis of the force gradient approach, by simply using the above described capacitance expressions (Eqs. (4)–(6)) to obtain the real and imaginary parts of the detected force gradient. Therefore, the second derivative of the total capacitance can be used to estimate the frequency shift

$$\Delta f = -\frac{1}{4} \cdot f_0 \cdot k^{-1} \cdot \frac{\partial^2 C}{\partial z^2} \cdot V^2. \tag{9}$$

Electrical phase can be then obtained in the same way as in the force approach, by calculating the imaginary to real signal ratio. Figure 7 shows LDS predictions (based on the previously obtained parameters) for PVAc film thicknesses ranging from 10 nm to 10 μm. As before, apex and cantilever contributions to the signal are shown in red and green lines, respectively, while total signal is shown with a blue (dashed) line.

In this case, cone and cantilever imaginary contributions are negligible even at relatively large thicknesses (until 5–6 μm). This effect is directly related with the second derivative of capacitance, due to the fact that both contributions hardly change at low-medium z values. It is also interesting to analyze the peak maximum frequency obtained by LDS as a function of thickness (Figure 6). As in the force approach, there is a clear initial shift to lower frequencies as thickness increases. This tendency is also reverted at high thicknesses (of about 4000 nm), until the original f_{max} is recovered. It is worth noticing that this effect is slightly different than in force mode, as also shown in Figure 6. In particular, the thickness dependence minimum appears to the right of the force approach (i.e., at higher thicknesses) and it is more pronounced (there is a decrease of about 250 Hz, while in force this decrease is of about 220 Hz). These force gradient approach results arise from the second derivative of the capacitance, which filters the cantilever imaginary contribution even at high thicknesses.[18]

3. Increasing force mode sensitivity

According to our previous analysis (see Sec. IV B 1), in order to gain sensitivity in the force mode method, the cantilever contribution to the measured force has to be substantially reduced. Figure 5 shows that for polymer film thicknesses of about 100 nm there is a relative maximum in the electrical phase peak intensity. At this particular thickness, the cantilever contribution represents about 61% of the real part of the signal, whereas that of the apex amounts to about 39%, being the contribution from the cone negligible (in the proposed model the cone nearest segments contribution is screened by the apex, while the upper cone segments are, like cantilever, far from the lower electrode). Moreover, the contribution of the cantilever to the imaginary part of the force is negligible, which in turn results in a large reduction

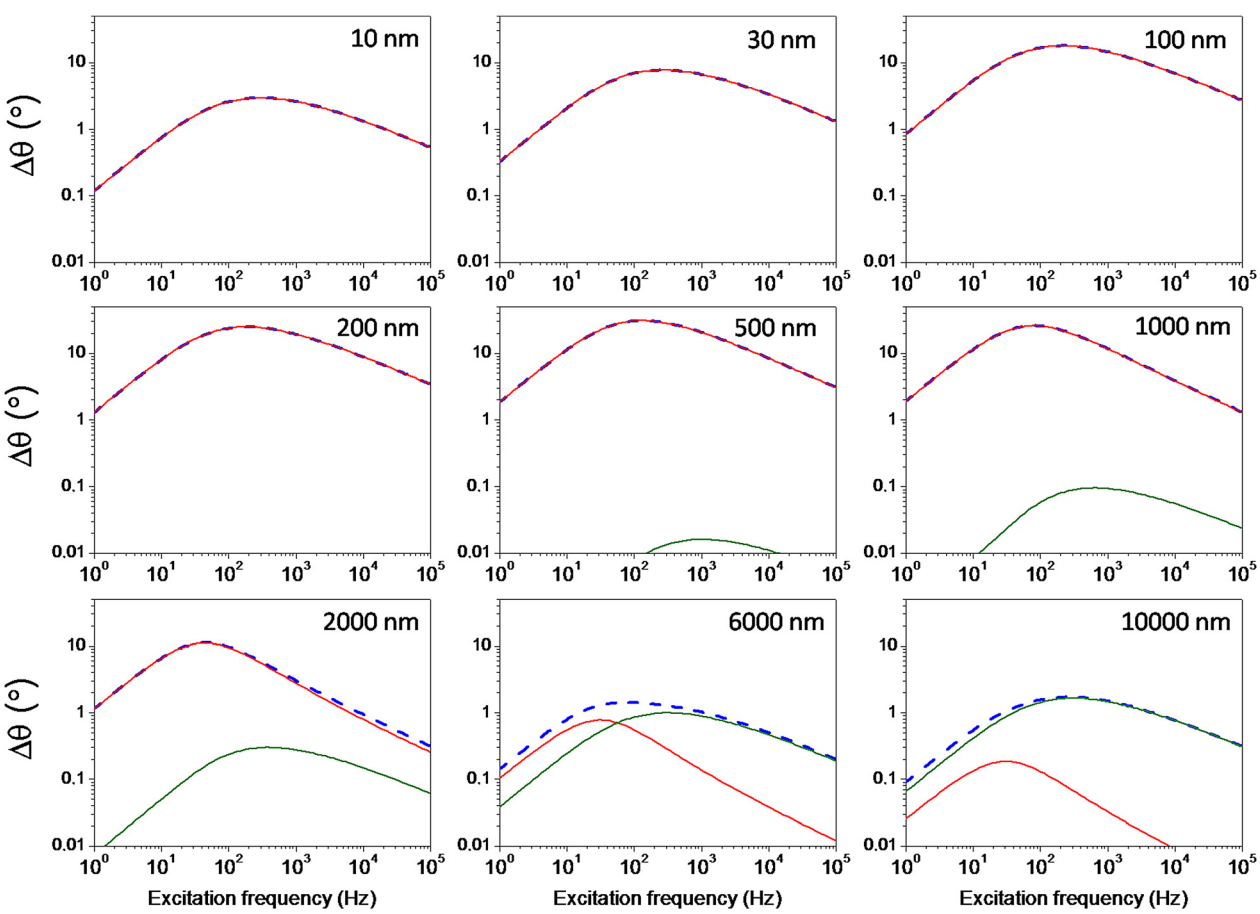

FIG. 7. Electrical phase (force gradient approach) predicted by the model for different polymer thicknesses. Apex and cantilever contributions to the signal are shown as red and green lines, respectively, while total signal is shown in blue (dashed line).

[This article is copyrighted as indicated in the article. Reuse of AIP content is subject to the terms at: http://scitation.aip.org/termsconditions. Downloaded to] IP: 161.111.180.191 On: Mon, 29 Sep 2014 09:04:52

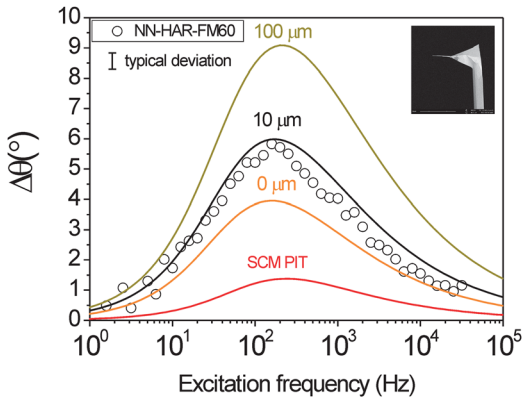

FIG. 8. *n*DS spectra on a PVAc film (thickness 100 nm) obtained with a NN-HAR-FM60 probe (empty circles). The inset shows the needle length (SEM) of about 10 μm. The red line stand for the electrical phase shift intensity predicted by the model for a SCM PIT of radius 25 nm. Lines for 100, 10, and 0 μm stand for the model prediction for probes with these particular needle lengths.

of the measured phase value. Since in the parallel plate capacitor approximation, the derivative of the capacitance responsible for the force depends significantly on the cantilever sample distance, the phase output in the force mode method should be quite sensitive to an increase of the cantilever/sample distance. In this regard, the use of especially designed AFM probes providing a larger cantilever/-sample distance appears to be a very promising approach. Commercial AFM probes providing larger cantilever/sample distances already exist, like those manufactured by Nauganeedles (NN-HAR-FM60, needle probe) consisting of a conductive needle of about 10 μm at the end of the cone with an apex radius of about 60 nm. Figure 8 shows *n*DS spectra acquired by using these new probes on a PVAc film with thickness of about 100 nm. As expected, a significantly higher phase shift peak value is obtained. By means of the proposed model, we have calculated the expected phase shift peak for a probe with this geometry that indeed accounts quite well for the measured values. The calculated cantilever contribution is now about 32%. Note that the phase shift increment arises from two factors, a larger tip radius (which enhances the relevance of the apex contribution) and a larger cantilever/sample distance (which results in a decrease of the cantilever contribution). In order to analyze the relevance of these two effects, we have calculated the expected signal for a conventional probe of the same apex radius (60 nm). As shown in Figure 8, the resulting spectrum shows a phase shift peak of about 4° which is about two times higher than that of a 25 nm radius probe. However, the spectrum is still below the experimentally obtained spectrum for the needle probe, indicating that part of the increment is related with the larger cantilever-sample distance. The model also allowed us to calculate the expected phase signal for a non conventional probe with much larger needle (c.a. 100 μm length) resulting in a larger phase shift peak. It is noteworthy that working with such a probe would not be easy due to the fact that the presence of a long needle also increases the mechanical vibrations and the dispersion of the data.

According to the previous results, the use of dedicated probes providing large distances between sample surface and cantilever is an efficient way to increase the sensitivity in force mode operation. Furthermore, this approach can be used without any change in the setup and consequently the broad frequency range is still fully available. However, using such kind of probes can introduce a larger sensitivity to mechanical vibrations which in turn would produce a reduction of the signal to noise ratio. Alternatively, other promising approach to increase the phase shift sensitivity in force mode operation is the shielding of the AFM probe cantilever, i.e., using probes with an excitable apex and a grounded cone/-cantilever, in order to remove parasitic capacitances contributing to the measured electrical force. In such experiments, the contributions from cone/cantilever would be completely negligible, thus maximizing sensitivity even for small apex radius, i.e., maintaining the spatial resolution. So by using force mode operation, it would be possible to detect a signal similar to that obtained using force gradient operation but without the restrictions imposed by the required electronics.

V. CONCLUSIONS

A physical model relating the phase shift signal of AFM based dielectric spectroscopy with the dielectric properties of a given material is proposed. This model is based on physically meaningful parameters, directly related to the AFM probe dimensions and the employed experimental setup. We have checked that by this modeling a quantitative description of the experimental results is possible, thus providing the way of obtaining quantitative material properties from *n*DS experiments. Furthermore, the modeling allowed us to determine the modifications of the experimental setup that will results in a significant improvement in the sensitivity of the force mode operation.

ACKNOWLEDGMENTS

We acknowledge the financial support provided by the Basque Country Government (IT-654-13) and the Spanish Ministry of Science and Innovation (MAT2012-31088). Financial support from EU-funded "European soft matter infrastructure" (reference 262348 ESMI) is also acknowledged.

APPENDIX: TECHNICAL INFORMATION

1. Experimental details

a. Samples

Polymer films of polyvinilacetate (PVAc) homopolymer (MW = 83 000 g/mol) were prepared by spin-coating polymer-toluene solutions onto a gold sputtered glass, which in turn was mounted on metallic disks of 12 mm diameter. Thicknesses of about 350–400 nm were obtained by using a 4 wt. % PVAc/toluene solution.

b. BDS

BDS measurements were performed on disc shaped samples with a diameter of 20 mm and a thickness of about 0.1 mm. Broadband high-resolution dielectric spectrometer

[This article is copyrighted as indicated in the article. Reuse of AIP content is subject to the terms at: http://scitation.aip.org/termsconditions. Downloaded to] IP: 161.111.180.191 On: Mon, 29 Sep 2014 09:04:52

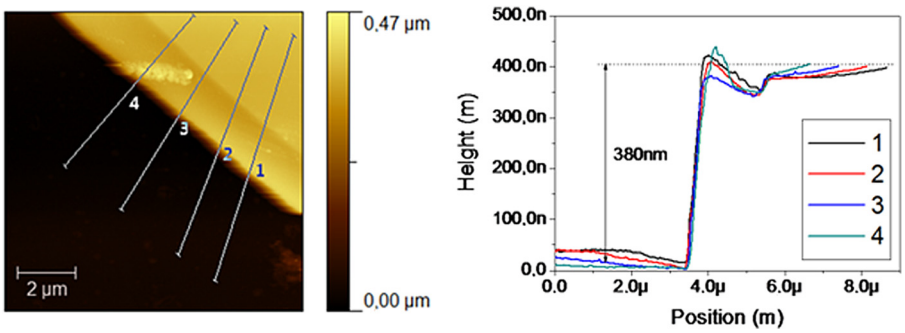

FIG. 9. Determination of the polymer thickness by using the scratch method. Left: AFM topography image (the lines stand for the profile determination paths). Right: Height as a function of the position.

(Novocontrol Alpha) was used to measure the complex dielectric permittivity in the frequency range from 10^{-2} to 10^{6} Hz. The sample temperature was controlled by nitrogen gas flow which enables temperature stability of about ± 0.1 K.

c. AFM general setup

Topography and mechanical phase images were simultaneously obtained in moderate tapping mode, with an Atomic Force Microscope MultiMode 8 (Bruker). The measurements were performed using Antimony (Sb) doped Si cantilevers, coated with Pt/Ir (SCM-PIT Bruker). Nominal values for the natural frequency (f_0), apex radius (R), and cantilever spring constant (k) for the probes are 75 kHz, 20 nm, and 1.5–3 N/m, respectively. Proof of concept experiments were conducted by using gold coated NN-HAR-FM60 AFM probes (Nauganeedles). Nominal f_0, R, and k values for these probes are 60 kHz, 50 nm, and 3 N/m, respectively.

During AFM measurements, sample temperature was controlled (from room temperature up to 150 °C) by using a Thermal Applications Controller (TAC, Bruker). A silicone cap was used as sealing to improve the thermal stabilization of the system. The atmosphere inside the silicon cap was controlled by using a dry nitrogen flow. An external LIA, Stanford Research SR830 (frequency range up to 100 kHz) was employed for EFM measurements.

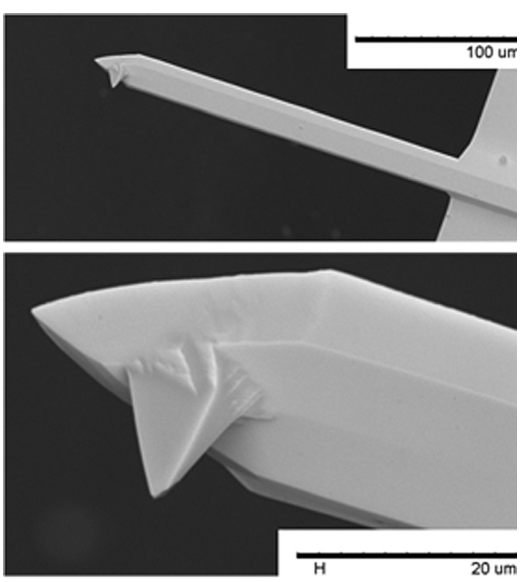

FIG. 10. SEM images of the conductive AFM probes (SCM PIT, Bruker).

d. nDS

Both electric phase and RMS amplitude were recorded using a homemade LabVIEW routine. As previously mentioned, a reference experiment was performed over a gold substrate without any polymer on it, (θ_{ref}). Dielectric spectra were obtained by evaluating the phase shift ($\Delta\theta$), i.e., $\Delta\theta = \theta_{ref} - \theta$, as a function of electrical excitation frequency.

2. Geometrical parameters

As shown in Figure 9, thickness measurements were performed by AFM after scratching the sample film with a sharp object.

As shown in Figure 10, the cantilever length and width were found to be about 250 μm and 30 μm (SEM). A cone height of 12 μm and an angle of 15° were also determined by SEM. On the other hand, tip sample distance was independently measured by using the AFM. In this case, the probe was kept at 0 nm (LSH = 0 nm) from the sample after engaging. Then, the oscillation amplitude was gradually increased until the resonance peak was truncated. As a result, by assuming that the maximum achieved oscillation amplitude (before affecting the resonance peak) is equal to the tip sample distance in rest, it is possible to obtain the typical tip-sample distance during experiments.

[1]F. Kremer and A. Schonhals, *Broadband Dielectric Spectroscopy* (Springer-Verlag, New York, 2003).
[2]Y. Martin, C. C. Williams, and H. K. Wickramasinghe, J. Appl. Phys. **61**, 4723 (1987).
[3]J. Tamayo and R. García, Langmuir **12**, 4430 (1996).
[4]G. Paul, Nanotechnology **12**, 485 (2001).
[5]C. Riedel, R. Arinero, P. Tordjeman, M. Ramonda, G. Lévêque, G. A. Schwartz, D. G. De Oteyza, A. Alegria, and J. Colmenero, J. Appl. Phys. **106**, 024315 (2009).
[6]L. Fumagalli, G. Gramse, D. Esteban-Ferrer, M. A. Edwards, and G. Gomila, Appl. Phys. Lett. **96**, 183107 (2010).
[7]C. Riedel, R. Arinero, P. Tordjeman, G. Lévêque, G. A. Schwartz, A. Alegría, and J. Colmenero, Phys. Rev. E **81**, 010801 (2010).
[8]C. Riedel, A. Alegria, G. A. Schwartz, R. Arinero, J. Colmenero, and J. J. Saenz, Appl. Phys. Lett. **99**, 023101 (2011).
[9]L. A. Miccio, M. M. Kummali, P. E. Montemartini, P. A. Oyanguren, G. A. Schwartz, Á. Alegría, and J. Colmenero, J. Chem. Phys **135**, 064704 (2011).
[10]C. Riedel, A. Alegría, G. A. Schwartz, J. Colmenero, and J. J. Sáenz, Nanotechnology **22**, 285705 (2011).
[11]P. S. Crider, M. R. Majewski, J. Zhang, H. Oukris, and N. E. Israeloff, Appl. Phys. Lett. **91**, 013102 (2007).

[This article is copyrighted as indicated in the article. Reuse of AIP content is subject to the terms at: http://scitation.aip.org/termsconditions. Downloaded to] IP: 161.111.180.191 On: Mon, 29 Sep 2014 09:04:52

[12]M. Labardi, D. Prevosto, K. H. Nguyen, S. Capaccioli, M. Lucchesi, and P. Rolla, in *Local Dielectric Spectroscopy of Nanocomposite Materials Interfaces, 2010* (AVS), p. C4D11.
[13]C. Riedel, R. Sweeney, N. E. Israeloff, G. A. Schwartz, R. Arinero, P. Tordjeman, G. Lévêque, A. Alegría, and J. Colmenero, Appl. Phys. Lett. **96**, 213110 (2010).
[14]T. P. Corrales, D. Laroze, G. Zardalidis, G. Floudas, H.-J. Butt, and M. Kappl, Macromolecules **46**, 7458 (2013).
[15]G. A. Schwartz, C. Riedel, R. Arinero, P. Tordjeman, A. Alegría, and J. Colmenero, Ultramicroscopy **111**, 1366 (2011).
[16]M. M. Kummali, L. A. Miccio, G. A. Schwartz, A. Alegría, J. Colmenero, J. Otegui, A. Petzold, and S. Westermann, Polymer **54**, 4980 (2013).
[17]S. Hudlet, M. Saint Jean, C. Guthmann, and J. Berger, Eur. Phys. J. B: Condens. Matter Complex Syst. **2**, 5 (1998).
[18]A. Gil, J. Colchero, J. Gómez-Herrero, and A. M. Baró, Nanotechnology **14**, 332 (2003).
[19]L. Fumagalli, G. Ferrari, M. Sampietro, and G. Gomila, Appl. Phys. Lett. **91**, 243110 (2007).
[20]G. Gomila, J. Toset, and L. Fumagalli, J. Appl. Phys. **104**, 024315 (2008).
[21]G. M. Sacha and J. J. Saenz, Appl. Phys. Lett. **85**, 2610 (2004).
[22]L. Fumagalli, G. Ferrari, M. Sampietro, and G. Gomila, Nano Lett. **9**, 1604 (2009).
[23]S. Magonov and J. Alexander, Beilstein J. Nanotechnol. **2**, 15 (2011).
[24]H. Nishiyama and M. Nakamura, IEEE Trans. Compon., Packag., Manuf. Technol., Part A **17**, 477 (1994).
[25]R. García, *Amplitude Modulation Atomic Force Microscopy* (WILEY-VCH, Weinheim, 2010).
[26]H. K. Nguyen, D. Prevosto, M. Labardi, S. Capaccioli, M. Lucchesi, and P. Rolla, Macromolecules **44**, 6588 (2011).
[27]H. K. Nguyen, M. Labardi, S. Capaccioli, M. Lucchesi, P. Rolla, and D. Prevosto, Macromolecules **45**, 2138 (2012).
[28]V. M. Boucher, D. Cangialosi, A. Alegría, and J. Colmenero, Phys. Rev. E **86**, 041501 (2012).
[29]H. Yin, S. Napolitano, and A. Schönhals, Macromolecules **45**, 1652 (2012).
[30]S. Havriliak and S. Negami, J. Polym. Sci., Part C: Polym. Symp. **14**, 99 (1966).
[31]M. Tyagi, A. Alegría, and J. Colmenero, J. Chem. Phys. **122**, 244909 (2005).
[32]G. A. Schwartz, E. Tellechea, J. Colmenero, and Á. Alegría, J. Non-Cryst. Solids **351**, 2616 (2005).

[This article is copyrighted as indicated in the article. Reuse of AIP content is subject to the terms at: http://scitation.aip.org/termsconditions. Downloaded to] IP: 161.111.180.191 On: Mon, 29 Sep 2014 09:04:52